

**FACULTY
OF MATHEMATICS
AND PHYSICS**
Charles University

BACHELOR THESIS

Andrej Rendek

**Simulations of dynamics of ultra-cold
quantum plasma**

Department of Surface and Plasma Science

Supervisor of the bachelor thesis: Mgr. Michal Hejduk, Ph.D.

Study programme: Physics

Study branch: Physics

Prague 2022

I declare that I carried out this bachelor thesis independently, and only with the cited sources, literature and other professional sources. It has not been used to obtain another or the same degree.

I understand that my work relates to the rights and obligations under the Act No. 121/2000 Sb., the Copyright Act, as amended, in particular the fact that the Charles University has the right to conclude a license agreement on the use of this work as a school work pursuant to Section 60 subsection 1 of the Copyright Act.

In date
Author's signature

A would like to show my appreciation for...

Title: Simulations of dynamics of ultra-cold quantum plasma

Author: Andrej Rendek

Department: Department of Surface and Plasma Science

Supervisor: Mgr. Michal Hejduk, Ph.D., Department of Surface and Plasma Science

Abstract: We investigate the confinement of charged particles in an oscillating electromagnetic field, intending to trap electrons and calcium ions simultaneously. The theoretical part of this thesis focuses on the derivation of exact and effective equations of motion in a single frequency quadrupole trap. We show a general treatment of stability in such a field. Passing attained knowledge onto two-frequency trapping, which is much more suitable for confining two species with widely different charge-to-mass ratios. We follow up by studying the stability of electrons, employing computer simulations in the ideal two-frequency Paul trap. Our ambition is to identify a stable configuration minimizing electrons' temperature. We create multiple ion Coulomb crystals and examine the effect of their presence on electrons' stability. These efforts support the development of an experiment with the ambition to create and study quantum plasma. The composition of this experiment is outlined here as well.

Keywords: Ion trapping, Coulomb crystal, Two frequency Paul trap

Contents

Introduction	3
1 Theoretical introduction	5
1.1 Coulomb crystal	5
1.1.0.1 Plasma	5
1.2 Ion trapping	6
1.2.1 Equation of motion	6
1.2.2 Effective potential	7
1.2.3 Adiabacity	9
1.2.4 Trap geometry	10
1.2.4.1 Multipole trap	10
1.2.4.1.1 Ideal quadrupole trap	12
1.2.4.2 Real geometry of our trap	13
1.2.5 Spring constant	13
1.2.6 Mathieu equation	14
1.2.7 Stability	15
1.3 Laser cooling	16
1.4 Design of the experiment	16
2 Co-trapping of two different species	19
2.1 Two frequency quadrupole Paul trap	19
2.2 Floquet theory	21
2.3 Simulation	23
2.3.1 Choice of time-step	27
2.3.2 Treatment of laser cooling	27
2.3.3 Simulating Coulomb crystal	27
2.3.4 The code	28
3 Results and discussion	29
3.1 Characteristics of $q_1 - q_2$ stability diagrams for one electron . .	29
3.2 Creating a Coulomb crystal	37

3.3	Stability of electron in Coulomb crystal	37
3.4	Future	38
Conclusion		39
Bibliography		41
A Using software		43
A.1	Python script	43

Introduction

This thesis' practical aim is to contribute to developing an experiment initiated by my supervisor Mgr. Michal Hejduk, Ph.D. In this experiment, we wish to create and study the properties of a quite unusual type of matter, Coulomb crystal (CC). CCs are mostly stationary structures of ions characterized by large coupling parameter Γ^1 , representing the ratio between electrostatic and kinetic energy of ions. These structures have been extensively studied now for decades. Our ambition is to introduce electrons to such a crystal and cool everything down. We will be aiming for sub-kelvin temperatures when electrons' de Broglie wavelength would be greater than the distance between them, forming so-called Fermi gas, which up to the current date, has not been achieved yet inside a CC. Creating a CC means confining a certain number of charged particles in bounded space. The first thing standing in our way is Earnshaw's theorem [1], stating that there is no stable electrostatic configuration of charged particles. Not feeling like giving up, we must try our chances outside the realm of electrostatics. Here we are already presented with two well-established ways of storing charged particles. One utilizes an axial magnetic field to confine particles in a radial direction and a static electric field for confinement in an axial direction. This approach developed by H.G. Dehmelt is called the Penning trap. The second option to restrict the movement of charged particles in all directions is to use the dynamic and static electric fields solely. The Pioneer of this technique was Wolfgang Paul. Both these gentlemen were awarded a shared Nobel prize for physics in 1989 for their efforts in this field. The ions in our experiment will be laser-cooled, which would be disturbed by a magnetic field due to Zeeman splitting. Ergo, we chose the latter method since we would otherwise need an unnecessarily complicated laser apparatus. Our job is to make a computer simulation of an ion crystal with electrons inside a Paul trap, optimizing its parameters to attain the lowest possible temperature of electrons, hopefully reaching the electron delocalization over multiple ions in the CC. The objectives of this thesis might be summed up as follows:

¹All the non-trivia will be further explained in the first chapter

- Development of a computer model simulating the motion of charged particles in the trap.
- Trap parameters optimization with the prospect of minimizing electron temperature.
- Real trap design suggestion.

Chapter 1

Theoretical introduction

In this chapter, we introduce concepts essential for understanding this thesis' concerns. The first subsection is aimed to deliver the basic characterization of CCs. In the following subsection, we talk about the motion of a charged particle in rapidly changing fields. Next, we will introduce the idea of laser cooling. And finally, in the last subsection, we propose our design of an experiment capable of achieving simultaneous electron-ion trapping and cooling.

1.1 Coulomb crystal

Most of the solid matter we come across has either a crystal or rather polycrystal structure. Meaning its elementary constituents (atoms, molecules, ions) create an ordered formation repeating itself, in the case of crystals up to macroscopic scales. The shape of these structures [2] is essentially dictated by the atomic wave function overlap. A CC orders itself differently. An average distance between ions in a CC is usually [3] five orders of magnitude larger than it is for atoms in typical matter. On this scale are quantum effects negligible, and ions are merely pushed away from each other by classical Coulomb interaction. Therefore they need an external force to keep them together, which is provided by a trapping potential in our case. However, these structures can also be found in nature, namely in the cores of white dwarfs and crusts of neutron stars.

1.1.0.1 Plasma

Not all texts agree on a precise definition of plasma. A somewhat broad definition [4] states that plasma is an ionized gas exerting collective behavior. We often demand quasineutrality as well, suggesting similar ion and electron concentrations. By this merit, a CC can not be labeled plasma as it is composed exclusively

of positive ions. Collective behavior means the plasma responds to external macroscopic stimuli as a whole. The standard parameter linked to this aspect is plasma frequency ω_p , describing how quickly plasma reacts to the imposed electromagnetic field.

$$\omega_p = \frac{nQ^2}{\varepsilon_0 M}, \quad (1.1)$$

where n represents a concentration of charged particles, Q their charge, M their mass, and ε_0 is the vacuum permittivity. This equation (1.1) shows that the electrons play an essential role in collective behavior, as they can react much more swiftly than heavy ions. That is another reason it is necessary to add electrons so that CC can become plasma.

Plasma can have multiple components, each having different masses and velocities. We define a temperature [4] for each species individually as their mean kinetic energy:

$$k_b T_s = \frac{1}{3} M_s \langle v_s^2 \rangle, \quad (1.2)$$

where $\langle v_s \rangle$ denotes an average velocity of single species, and k_b is a Boltzmann constant.

Another crucial attribute when examining plasma is the Γ parameter, representing the proportion of Coulomb potential energy to the plasma's kinetic energy.

$$\Gamma \equiv \frac{E_c}{k_b T}, \quad (1.3)$$

where T denotes temperature, and E_c Coulomb energy. It is not easy to figure out the potential energy of a general plasma. However, when dealing with Coulomb crystals composed of tens to hundreds of ions, nothing stops us from computing it exactly. Classical thermal plasma has $k_b T \gg E_c$. In the case of CCs, $k_b T < E_c$ and we are talking about *strongly coupled* plasma.

1.2 Ion trapping

Here we introduce the concept of trapping a single ion by a quickly oscillating field. We will tightly follow a classic textbook [5] in the whole section, starting by writing the equation of motion.

1.2.1 Equation of motion

Let us consider a particle with mass M , charge Q , and position denoted by vector \mathbf{r} . We insert such a particle into the external time-dependent electromagnetic

field described by $\mathbf{E}(t, \mathbf{r})$ and $\mathbf{B}(t, \mathbf{r})$. The Lorentz force gives us the equation of motion:

$$M\ddot{\mathbf{r}} = Q[\mathbf{E}(t, \mathbf{r}) + \dot{\mathbf{r}} \times \mathbf{B}(t, \mathbf{r})]. \quad (1.4)$$

Since we are not using any external magnetic field, and while trapping a particle in a compact space, we usually deal with small velocities. Therefore we can neglect¹ the effect of the term $\dot{\mathbf{r}} \times \mathbf{B}$, which means that the equation of motion simplifies to:

$$M\ddot{\mathbf{r}} = Q\mathbf{E}(t, \mathbf{r}). \quad (1.5)$$

We further assume that the electric field is composed of static and time-dependent parts. We are looking for a simple periodic time-dependency. A typical way to model such behavior would be $\mathbf{E}(t) \sim \cos(\Omega_1 t)$, giving us:

$$\mathbf{E}(t, \mathbf{r}) = \mathbf{E}_s(\mathbf{r}) + \mathbf{E}_0(\mathbf{r}) \cos(\Omega_1 t), \quad (1.6)$$

and following equation of motion:

$$M\ddot{\mathbf{r}} = Q[\mathbf{E}_s(\mathbf{r}) + \mathbf{E}_0(\mathbf{r}) \cos(\Omega_1 t)]. \quad (1.7)$$

1.2.2 Effective potential

Dealing with such (1.7) rapidly changing non-autonomous differential equations can be a riot, although it is possible to solve them analytically for special boundary conditions, as will be discussed further. By a lucky chance, we are not always interested in exact solutions while trapping ions. The relevance often lies in the time-averaged effect of a swiftly changing field. With that in mind, we will try to derive *effective potential* fulfilling precisely this role.

Let's consider initial conditions: $\mathbf{r}(0) = \mathbf{r}_0$ and $\dot{\mathbf{r}}(0) = 0$. For the case of an oscillating electric field with homogeneous amplitude $\mathbf{E}_0(\mathbf{r}) = \text{const}$, we obtain a trivial solution:

$$\mathbf{r}(t) = \mathbf{r}_0 - \mathbf{A} \cos(\Omega_1 t), \quad (1.8)$$

where the vector:

$$\mathbf{A} \equiv \mathbf{A}(\mathbf{r}) = \frac{QE_0(\mathbf{r})}{m\Omega_1^2}, \quad (1.9)$$

is an amplitude of oscillation around the initial position of the particle. The crucial consequence of this result is that we can further restrict the motion of a particle by increasing the frequency of field oscillation. Of course, the situation changes when we bring a small inhomogeneity into the field. Here comes our first leap of fate by assuming that our defining relation for the amplitude of oscillation (1.9)

¹This and other approximations are further discussed in the section 2.3.

won't be affected by such inhomogeneity. Instead, the particle will drift slowly towards the weaker field region, minimizing its mean potential energy. Motivated by these two assumptions, we can try to find a solution to the equation of motion in the form:

$$\mathbf{r}(t) = \mathbf{R}_0(t) + \mathbf{R}_1(t), \quad (1.10)$$

where $\mathbf{R}_0(t)$ represents consequence of smooth drift and $\mathbf{R}_1(t)$ stands for rapid oscillation, expressed as:

$$\mathbf{R}_1(t) = -\mathbf{A} \cos(\Omega_1 t). \quad (1.11)$$

If the field amplitude $\mathbf{E}_0(\mathbf{r})$ varies smoothly with regards to the space dimension, we can get by just with its first-order Taylor expansion around \mathbf{R}_0 :

$$\mathbf{E}_0(\mathbf{R}_0(t) - \mathbf{A} \cos(\Omega_1 t)) \approx \mathbf{E}_0(\mathbf{R}_0(t)) - (\mathbf{A} \cdot \nabla) \mathbf{E}_0(\mathbf{R}_0(t)) \cos(\Omega_1 t) + \dots \quad (1.12)$$

Substituting (1.10) and (1.12) into equation of motion (1.7) (*omitting currently uninteresting static term \mathbf{E}_s*), we get:

$$M(\ddot{\mathbf{R}}_0(t) + \ddot{\mathbf{R}}_1(t)) = Q \cos(\Omega_1 t) [\mathbf{E}_0(\mathbf{R}_0(t)) - (\mathbf{A} \cdot \nabla) \mathbf{E}_0(\mathbf{R}_0(t)) \cos(\Omega_1 t)]. \quad (1.13)$$

Presuming slow spacial variation of vectorfield $\mathbf{E}_0(\mathbf{r})$ implies:
 $|\ddot{\mathbf{A}}| \ll |\dot{\mathbf{A}}|\Omega_1 \ll |\mathbf{A}|\Omega_1^2$, which we can exploit in time derivative of quickly oscillating term $\mathbf{R}_1(t)$ (1.11), giving us:

$$\ddot{\mathbf{R}}_1 = -\ddot{\mathbf{A}} \cos(\Omega_1 t) + 2\Omega_1 \dot{\mathbf{A}} \sin(\Omega_1 t) + \mathbf{A}\Omega_1^2 \cos(\Omega_1 t) \approx \mathbf{A}\Omega_1^2 \cos(\Omega_1 t) \quad (1.14)$$

Further substituting for amplitude of oscillation \mathbf{A} from (1.9) continuing in the spirit of time-averaging:

$$\mathbf{A} = \frac{q\mathbf{E}_0(\mathbf{r})}{M\Omega_1^2} \approx \frac{q\mathbf{E}_0(\mathbf{R}_0(t))}{M\Omega_1^2}, \quad (1.15)$$

which transfers into \mathbf{R}_1 as:

$$\mathbf{R}_1(t) = -\frac{Q\mathbf{E}_0(\mathbf{R}_0(t))}{M\Omega_1^2} \cos(\Omega_1 t). \quad (1.16)$$

Terms in the equation of motion with dependence on $\cos(\Omega_1 t)$ cancel each other out and by using a vector identity:

$$(\mathbf{E}_0 \cdot \nabla) \mathbf{E}_0 = \frac{1}{2} \nabla E_0^2 - \mathbf{E}_0 \times (\nabla \times \mathbf{E}_0) = \frac{1}{2} \nabla E_0^2, \quad (1.17)$$

where the second equality follows from Maxwell equation for quasistatic field: $\nabla \times \mathbf{E}_0 = 0$. By replacing term $\cos^2(\Omega_1 t)$ with its mean value $\langle \cos^2(\Omega_1 t) \rangle = 1/2$ we finally obtain:

$$M\ddot{\mathbf{R}}_0 = \frac{Q^2}{4M\Omega_1^2} \nabla E_0^2. \quad (1.18)$$

Now by resurrecting the static field term as $\mathbf{E}_s = -\nabla\Phi_s$, we can define the effective potential:

$$V^*(\mathbf{R}_0) = \frac{Q^2 E_0^2(\mathbf{R}_0)}{4M\Omega_1^2} + Q\Phi_s, \quad (1.19)$$

describing the time-averaged force on a charged particle:

$$M\ddot{\mathbf{R}}_0 = -\nabla V^*(\mathbf{R}_0). \quad (1.20)$$

This equation is much easier to solve and discuss than the original equation of motion (1.7) as it does not involve any explicit time-dependency. After solving it, we can quickly obtain the term $\mathbf{R}_1(t)$ from (1.16) and get an approximative solution to the original equation of motion. From the Fourier analyses of numerically exact solutions [5] we know about the presence of higher-order terms:

$$\mathbf{r}(t) = \mathbf{R}_0(t) + \mathbf{R}_1(t) + \mathbf{R}_2(t) + \dots,$$

where $\mathbf{R}_2(t) + \dots$ are referred to as micro oscillations. We must be careful about keeping the space variation of $E_0(r)$ sufficiently small. Otherwise, these micro oscillations can become large enough to significantly disturb the trajectory of a particle.

1.2.3 Adiabacity

Let us further investigate the motion of a charged particle in derived effective potential. The first integral of the equation (1.20) is:

$$\frac{1}{2}MR_0^2 + \frac{Q^2E_0^2}{4M\Omega_1^2} + Q\Phi_s = E_m, \quad (1.21)$$

where $E_m = \text{const}$ is the total energy of a charged particle inside the trap. Furthermore, if we consider the average kinetic energy of the rapidly oscillatory motion:

$$\left\langle \frac{1}{2}MR_1^2 \right\rangle = \frac{1}{2}M \frac{Q^2E_0^2}{M^2\Omega^4} \Omega^2 \langle \sin^2(\Omega t) \rangle = \frac{Q^2E_0^2}{4M\Omega_1^2}, \quad (1.22)$$

we see that equation (1.21) implies:

$$\frac{1}{2}MR_0^2 + \left\langle \frac{1}{2}MR_1^2 \right\rangle + Q\Phi_s = E_m, \quad (1.23)$$

which means that if the necessary assumptions in the derivation of the effective potential are met, then the total time-averaged energy of the system is an adiabatic constant. Such an outstanding finding provokes a question of whether we can identify a range of validity for the effective potential. There are more ways to approach this problem. We follow the one demonstrated in [5], kicking off the necessary condition for keeping just the first two terms in Taylor expansion (1.12) of the field $\mathbf{E}(\mathbf{r})$. This condition is satisfied if the spatial change of the field is much smaller than the field itself over the scope of one rapid oscillation, meaning:

$$|2(\mathbf{A} \cdot \nabla)\mathbf{E}_0| < |\mathbf{E}_0|. \quad (1.24)$$

Inspired by this condition we define a new parameter η :

$$\eta = \frac{|2(\mathbf{A} \cdot \nabla)\mathbf{E}_0|}{|\mathbf{E}_0|} = \frac{2Q|\nabla\mathbf{E}_0|}{M\Omega_1^2}, \quad (1.25)$$

where the last equality follows after implementing (1.9) and (1.17). We can use this parameter to check for the possibility of employing effective pseudopotential. Moreover, it can be a reliable indicator of stable trapping conditions.

1.2.4 Trap geometry

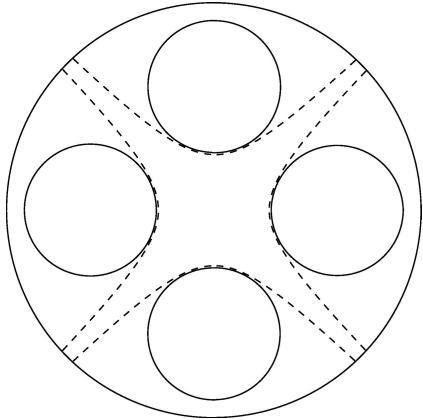
Previously derived equations indirectly feature the potential $\Phi = \Phi_{rf} + \Phi_s$ as the dynamic and static electric fields can be expressed as: $\mathbf{E}_0 \cos(\Omega_1 t) = -\nabla\Phi_{rf}$ and $\mathbf{E}_s = -\nabla\Phi_s$. So to give these general equations some concrete shape, we need to find this potential. In our quasistationary treatment of the electric field, it means solving the Laplace equation for a given boundary condition. Writing a general solution to the Laplace equation is possible only for certain symmetries. One such is cylindrical symmetry, for which we can work out the solution by hand using a Fourier method of separating variables in polar coordinates ($x = r \cos \varphi$, $y = r \sin \varphi$) as:

$$\Phi(r, \varphi) = C_0 + D_0 \ln(r) + \sum_{n \in \mathbb{N}} \left([A_n r^n + B_n r^{-n}] [C_n \sin(n\varphi) + D_n \cos(n\varphi)] \right), \quad (1.26)$$

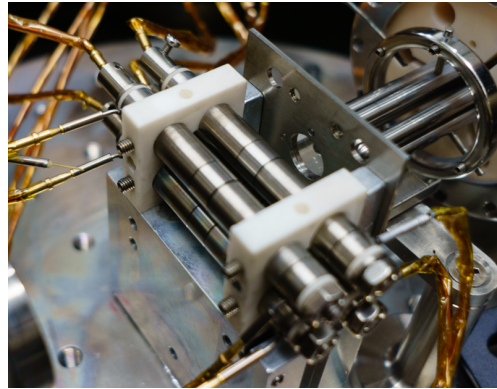
where C_0 , D_0 , A_n , B_n , C_n and D_n are coefficients that need to be determined from boundary conditions.

1.2.4.1 Multipole trap

A multipole is one of Paul trap's classical, well-studied geometries. N -th order multipole consists of $2n$ linear electrodes arranged with a discrete cylindrical symmetry.



(a) The scheme of quadrupole's cross-section. Adapted from [6].



(b) A photograph of linear quadrupole trap.

Figure 1.1 The quadrupole trap

In the figure 1.1a, we can see a comparison of a quadrupole trap's hyperbolical (*dashed*) and linear (*four circles*) electrode geometries. The quadrupole is already a very important geometry worth a special alias → the Paul trap, as will be pointed out shortly. We define a characteristic length of the multipole ℓ_0 , indicating the closest distance from the trap's center to an electrode. It is possible to obtain a potential of a multipole with infinitely long linear electrodes by applying boundary conditions (1.27) to a solution of Laplace equation with cylindrical symmetry (1.26).

Do I need to cite somebody
for 1.3b?

$$\Phi(r, \varphi)|_{r=0} = 0, \quad (1.27a)$$

$$\Phi(r, \varphi)|_{r=\ell_0} = \Phi_0 \cos(n\varphi), \quad (1.27b)$$

where $\Phi_0 = V_0 + V_1 \cos(\Omega_1 t)$ is a potential applied on electrodes. Most of the coefficients in (1.26) get wiped out, and we end up with the potential of n-th order multipole ($n > 0$) as:

$$\Phi(r, \varphi) = \Phi_0 \hat{r}^n \cos(n\varphi), \quad (1.28)$$

where $\hat{r} = r/\ell_0$. We get an electric intensity in polar coordinates as:

$$\mathbf{E}(r, \varphi) = -\nabla_{r\varphi}\Phi(r, \varphi), \quad (1.29)$$

where $\nabla_{r\varphi} = \left[\frac{\partial}{\partial r}, \frac{1}{r} \frac{\partial}{\partial \varphi} \right]^\top$. Hence:

$$\mathbf{E}(r, \varphi) = \frac{\Phi_0}{\ell_0} n \hat{r}^{n-1} \begin{bmatrix} -\cos(n\varphi) \\ \sin(n\varphi) \end{bmatrix}, \quad (1.30)$$

which in the Cartesian representation takes the form [5]:

$$\begin{bmatrix} E_x \\ E_y \end{bmatrix} = \frac{\Phi_0}{\ell_0} n \hat{r}^{n-1} \begin{bmatrix} -\cos((n-1)\varphi) \\ \sin((n-1)\varphi) \end{bmatrix}. \quad (1.31)$$

After substituting for Φ_0 we get equation of motion in variable $\hat{r} = [x/\ell_0, y/\ell_0]^\top$:

$$\frac{d^2 \hat{r}}{dt^2} + \frac{nQ}{M\ell_0^2} (V_0 + V_1) \cos(\Omega_1 t) \hat{r}^{n-1} \begin{bmatrix} -\cos((n-1)\varphi) \\ \sin((n-1)\varphi) \end{bmatrix} = \mathbf{0}. \quad (1.32)$$

We see that for the case $n = 2$ the equation of motion (1.32) is linear. The same is clearly does not hold for $n > 2$. That is why the motion in a quadrupole trap is the easiest to describe, and we chose this geometry to study simultaneous electron-ion trapping in this thesis.

1.2.4.1.1 Ideal quadrupole trap

We have already derived a equation of motion for single charged particle in a quadrupole trap $\rightarrow n = 2$ in (1.32). This equation gets further simplified by replacing linear electrodes with hyperbolical ones 1.1a. With this change, the electric field gets scaled [7] by a factor $1/2$, but foremost it loses the spatial dependence on the angle φ . In that case, the motion in the x and y directions stays independent, and we obtain an equation of motion in a variable $\mathbf{r} = [x, y]^\top$ for an idealized quadrupole trap:

$$M\ddot{\mathbf{r}} = -\frac{Q}{\ell_0^2} [V_0 + V_1 \cos(\Omega_1 t)] \mathbf{r}. \quad (1.33)$$

It is possible to assemble a Paul trap for confinement in all directions. In that case, the same equation also describes motion in the z-direction, but with a rescaled right-hand side by the factor of -2 . We will take a closer look at the equation (1.33) in the section 1.2.6. While we are at it, we can take a step back and define the potential for the idealized quadrupole trap. Equation of motion in terms of such potential would be: $M\ddot{\mathbf{r}}(t) = -Q\nabla V(t, \mathbf{r})$, comparing with the (1.33) gives us desired potential:

$$V(t, \mathbf{r}) = [V_0 + V_1 \cos(\Omega_1 t)] \frac{x^2 + y^2 - 2z^2}{2\ell_0^2}. \quad (1.34)$$

Another essential subject we are interested in is the effective potential for this geometry. For that, we need to evaluate for E_0 in the equation (1.19). The value of E_0 can be easily derived from (1.30), where for our case $\Phi_0 = V_1/2$, as:

$$E_0 = \frac{V_1}{\ell_0^2} \tilde{r}, \quad (1.35)$$

where we define $\tilde{\mathbf{r}} \equiv [x, y, -2z]^\top$. Meaning the effective potential for ideal Paul trap is:

$$V^*(\mathbf{r}) = \frac{Q^2 V_1^2}{4\ell_0^4 M \Omega_1^2} \tilde{r}^2 + Q\Phi_s = \frac{Q^2 V_1^2}{4\ell_0^4 M \Omega_1^2} (x^2 + y^2 + 4z^2) + Q\Phi_s. \quad (1.36)$$

1.2.4.2 Real geometry of our trap

Since we want to implement laser cooling in our experiment, the Paul trap is not a viable option, as its apparatus would stand in the way of laser beams. For this reason, we will use surface electrodes where the particles levitate above the trap so that the ions will be accessible to us.

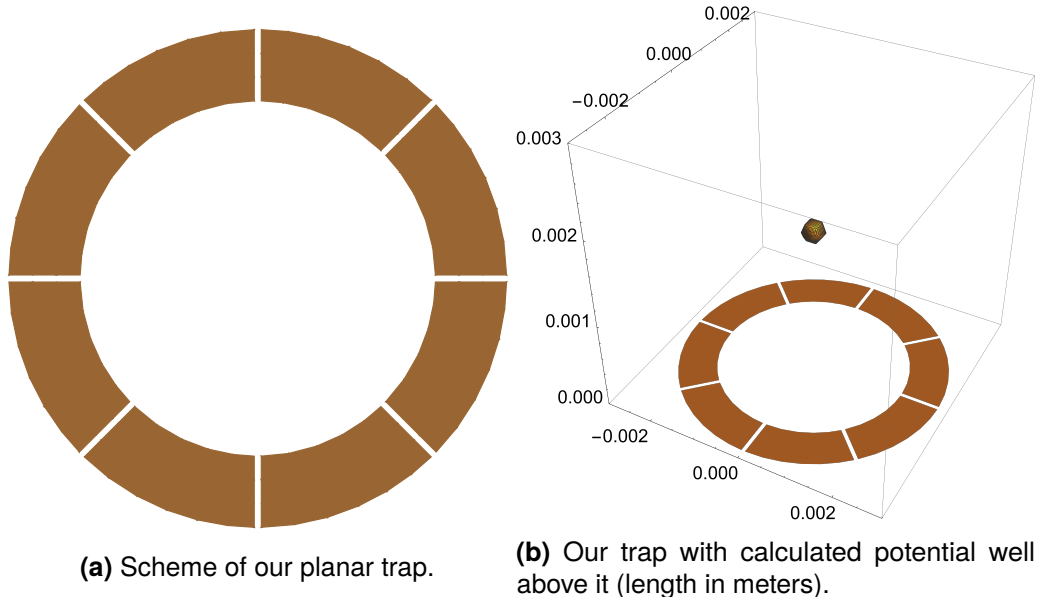


Figure 1.2 Planar trap geometry

Nevertheless, we will conduct our research in this thesis by examining the situation with the geometry of the 3D quadrupole trap with hyperbolic electrodes.

1.2.5 Spring constant

If we focus on the dynamic component of an effective potential (1.36), we can see that it is formally equivalent to a potential of a harmonic oscillator². This

²Meaning a potential in the form: $V(\xi) = \frac{\kappa}{2}\xi^2$

encourages us to define a spring constant:

$$\kappa \equiv \frac{Q^2 V_1^2}{2\ell_0^4 M \Omega_1^2}, \quad (1.37)$$

characterizing the strength of trapping potential. The spring constant is closely related to a frequency of oscillation in a harmonic potential. Such frequency is called secular, denoted:

$$\omega \approx \sqrt{\kappa/M} = QV_1/\sqrt{2}\ell_0^2 M \Omega_1. \quad (1.38)$$

The good news is that the spring constant does not depend on the charge sign, making it possible to trap electrons as well as ions. The bad news is that the spring constant depends on the charge-to-mass ratio Q/M , making it practically very difficult to trap electrons and ions simultaneously. For our case of trapping Ca^+ ions together with electrons, we get $\kappa_{\text{electron}}/\kappa_{\text{ion}} = M_{\text{ion}}/M_{\text{electron}} \approx 73000$ while we would like to achieve $\kappa_{\text{electron}}/\kappa_{\text{ion}} \sim 10$ so that electron trajectories would ideally stay inside the ion crystal but at similar scales. It seems that we have hit upon a huge snag with our approach. Fortunately, we do not have to abandon the discussed concept for trapping. We can instead improve on it by adding a second frequency. Such change allows us to treat both species' stability individually and makes it possible to manage the desired ratio of spring constants. Two frequency Paul trap will be further discussed in section 2.1.

1.2.6 Mathieu equation

Let us reexamine our original equation of motion (1.7) for the case of a quadrupole trap with ideal hyperbolical electrodes. After time transformation $\tau = \Omega_1 t/2$, the equation (1.33) molds into:

$$\ddot{\mathbf{r}}(\tau) = [a - 2q_1 \cos(2\tau)] \mathbf{r}, \quad (1.39)$$

where:

$$a = \frac{4QV_0}{M\ell_0^2\Omega_1^2}, \quad (1.40a)$$

$$q_1 = -\frac{2QV_1}{M\ell_0^2\Omega_1^2}. \quad (1.40b)$$

The equation (1.39) bears a name after E.L. Mathieu, who was the first to extensively study this ordinary differential equation(ODE) in the context of vibrating membranes. It has an analytical solution [8] in terms of special functions called

Mathieu functions, denoted ce_n and se_n , sometimes referred to as cosine-elliptic and sine-elliptic. The secular frequency is given by [5] the Dehmelt approximation:

$$\omega \approx \frac{\Omega_1}{2} \sqrt{a + \frac{q_1^2}{2}}. \quad (1.41)$$

If we do not apply any static field (*as in is the case for our configuration*) the secular frequency is:

$$\omega \approx \frac{\Omega_1}{2} \sqrt{\frac{q_1^2}{2}} = \frac{QV_1}{\sqrt{2}\ell_0^2 M \Omega_1}, \quad (1.42)$$

which is in accordance with the result we attained with the spring constant in the harmonic pseudopotential.

1.2.7 Stability

The stability of a linear system such as (1.39) can be examined with the help of a robust theory for linear ODEs with periodic coefficients, which we do in section 2.2. Nevertheless, we eventually want to study the trapping of multiple charged particles, and their mutual interaction razes the linearity of our equations. There is no single outright mathematical way to define the stability of a non-linear, non-autonomous system. Mathematical approaches might demand the boundedness of the solution in the phase space. Then we would talk about Lagrange stability [9]. Another approach would be to seek stable points and study what happens to the solutions starting in their proximity. This approach is referred to as Lyapunov stability [10]. We will use a simple but practical criterion for identifying stable solutions. A stable particle cannot vacate the internal dimension of the trap, meaning:

$$\max_{x \in \mathcal{L}}(r) \leq r_m < \ell_0, \quad (1.43)$$

where \mathcal{L} is the whole trajectory of the particle and r_m is maximal allowed distance from the center of a trap. The drawback of this definition is that we must keep the simulation going long enough to account for the slowly diverging particles, and we are yet to determine the value of r_m . However, we can also characterize the mode for stable confinement in a more general manner [5]. First, we limit ourselves to work within the condition for adiabaticity to ensure that the dynamic field does not continually augment the particle's energy. Then we can exploit the equation (1.23) in the following way. A stable particle must have no secular momentum $\dot{R}_0 = 0$ at the point r_m to avoid collision with the electrode. The effective potential near the electrode must be greater than the adiabatic constant E_m . Otherwise, the potential will not be powerful enough to prevent rapid oscillatory motion from

ejecting the particle out of the trap. Giving us the applicable inequality for stable confinement:

$$\frac{Q^2 E_0^2(r_m)}{4M\Omega^2} + Q\Phi_s > E_m. \quad (1.44)$$

We still need to find the right value for r_m . It has been established [5] that $r_m = 0.8 \ell_0$ accomplishes adiabaticity for most cases, which we will also use as a stability condition in our simulations:

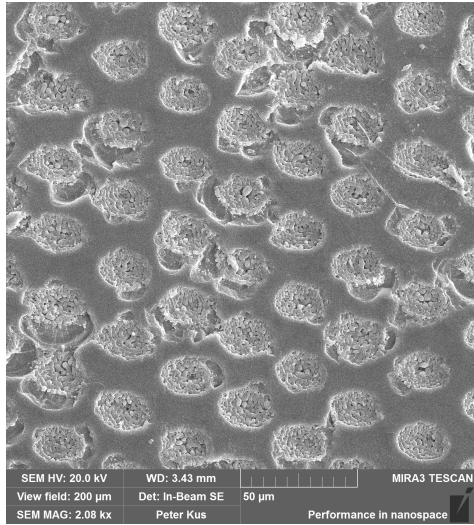
$$\max_{x \in \mathcal{L}}(r) \leq 0.8 \ell_0. \quad (1.45)$$

1.3 Laser cooling

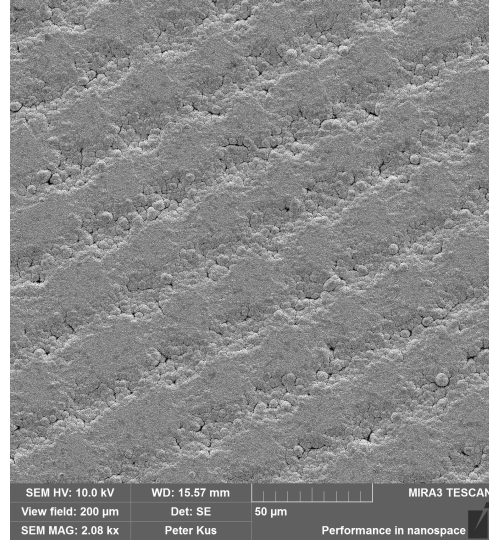
We demonstrate the principle of laser cooling on a calcium ion. The Ca^+ ion has an energy gap between the ground ($S_{1/2}$) and one of its excited ($P_{1/2}$) states with the value corresponding to the wavelength of 397 nm [11]. By tuning the wavelength of our laser slightly below this transition energy, we can exploit the Doppler effect so that only ions moving towards the laser can experience radiation with the right frequency to excite them. After a brief time, the atom will deexcite, emitting a photon in a random direction. The only way the ion would still have the same momentum as before the absorption is if the photon was emitted exactly in the same direction as it was absorbed (as if the photon did not interact with the atom at all). But since the photon emission is isotropic, the ion will effectively slow down. This type of laser cooling is also known as *Doppler cooling*. Detailed explanation can be found in [12].

1.4 Design of the experiment

As we have already stated, we chose a planar trap geometry, offering easy access to ions for laser cooling. Creating such a trap is a challenge in itself, and we have other colleagues in our team devoted to completing this task. Here we offer a quick overview of its development. Our circuit material is made of borosilicate glass for practical reasons. On it, we need to deposit a layer of copper by electroplating, forming the electrodes of our trap. Here arises the first problem, as the copper suffers from poor adhesion on the smooth surface of the glass. There are many ways to overcome this issue. We chose a straightforward one by roughening the glass mechanically with lasers.



(a) The surface of the glass after the laser roughening.



(b) A copper layer on the glass.

Figure 1.3 Pictures of our electrode manufacturing taken by an electron microscope.

We also use lasers to cut ways for the connection of each electrode to the power source. Next, we need a source of calcium ions. We manage that by evaporation from a calcium rod under a high voltage. Evaporated atoms will be excited by a 397 nm, laser creating a desired ion Ca^+ and an electron. For cooling, we use two lasers. The first is the same as we use for photo-ionization. The second with a wavelength of 866 nm is necessary for cooling to lower temperatures, exploiting another transition of calcium ion between the state ($P_{1/2}$) and the meta-stable state ($D_{3/2}$). Of course, such a complex experiment is met with dozens of other technical issues, but those are outside the scope of this thesis.

Chapter 2

Co-trapping of two different species

2.1 Two frequency quadrupole Paul trap

As was mentioned in the section 1.2.5, we can use two frequencies, each targeting to optimize the trapping of one species. Higher frequency Ω_2 for trapping electrons, with the potential V_2 applied to the electrode. A lower frequency Ω_1 with potential V_1 for trapping ions. We have already derived the ideal quadrupole potential for a single frequency case. Repeating the same process with the exception of using applied potential on the electrodes in the form $\Phi_0 = V_0 + V_1 \cos(\Omega_1 t) + V_2 \cos(\Omega_2 t)$, would yield two-frequency potential for an ideal quadrupole:

$$V(t, \mathbf{r}) = [V_0 + V_1 \cos(\Omega_1 t) + V_2 \cos(\Omega_2 t)] \frac{x^2 + y^2 - 2z^2}{2\ell_0^2}. \quad (2.1)$$

The equations of motion for a particle in such potential, after a change of variable: $\tau = t\Omega_2/2$ are:

$$\ddot{x}(\tau) = x(\tau) \left[a - 2q_1 \cos(2\tau\Omega_1/\Omega_2) - 2q_2 \cos(2\tau) \right], \quad (2.2a)$$

$$\ddot{y}(\tau) = y(\tau) \left[a - 2q_1 \cos(2\tau\Omega_1/\Omega_2) - 2q_2 \cos(2\tau) \right], \quad (2.2b)$$

$$\ddot{z}(\tau) = -2z(\tau) \left[a - 2q_1 \cos(2\tau\Omega_1/\Omega_2) - 2q_2 \cos(2\tau) \right], \quad (2.2c)$$

where a , q_1 and q_2 are dimensionless parameters:

$$a = 4 \frac{QV_0}{M\Omega_2^2 \ell_0^2}, \quad (2.3a)$$

$$q_1 = -2 \frac{QV_1}{M\Omega_2^2 \ell_0^2}, \quad (2.3b)$$

$$q_2 = -2 \frac{QV_2}{M\Omega_2^2 \ell_0^2}. \quad (2.3c)$$

Although we will not use any static potential in our case, we keep the term $\sim a$ for the generality of our equations.

Sometimes, instead of solving exact equations of motion, we can get along by simulating a charged particle in an effective potential, significantly reducing computational time. We will use this option for creating a Coulomb crystal. When trapping electrons, the condition (2.7) must be satisfied; hence we can use already derived single frequency effective potential (1.36):

$$V_{el}^*(r) = \frac{M_{el}\Omega_2^2 q_2^2}{16} (x^2 + y^2 + 4z^2), \quad (2.4)$$

where now, we have set the static field to zero and substituted for q_2 from (2.3c). In pseudopotential for ions, both frequencies will play their parts. Let us remark that Mathieu parameters (2.3) differ for the case of electron and ion by a factor of M_{el}/M_{ion} . Using the Mathieu parameters evaluated for electrons, the pseudopotential for ions [7] is:

$$V_{ion}^*(r) = \frac{M_{el}\Omega_2^2}{16M_{ion}} \left(\left(\frac{\Omega_2}{\Omega_1} \right)^2 q_1^2 + q_2^2 \right) (x^2 + y^2 + 4z^2). \quad (2.5)$$

We proceed by setting up a two-frequency trap as described in [13, 14]. First, we must acknowledge that while the higher frequency can only improve the stability of heavier ions, the slower field can easily misguide the electron. Such a latent instability is commonly anointed as the *parametric excitation*. We have to ensure that the trapping of electrons due to the higher frequency field is strong enough to withstand this undesirable effect. We can secure that to some extent by choosing potentials on electrodes in such a way that $V_1 \ll V_2$. We are able to provide potentials up to $V_2 \sim 100$ V, and $V_1 \sim 5$ V, in the conditions of our experiment. Let us now look at each frequency setup independently. Using (1.37), we get a ratio of spring constants:

$$K = \frac{\chi_{el}(\Omega_2)}{\chi_{ion}(\Omega_1)} \approx \frac{M_{ion}}{M_{el}} \left(\frac{V_2}{V_1} \frac{\Omega_1}{\Omega_2} \right)^2. \quad (2.6)$$

The correct way to create a stable configuration of a two-frequency trap is to begin by finding the optimal parameters for the confinement of the lighter species. Optimal trapping in a single frequency trap corresponds to [5] $q_2 \approx 0.4$. Using (2.3c), with the choice of $V_2 = 100$ V, we obtain optimal frequency for electron trapping as $\Omega_2 = 1.88 \times 10^{10}$ rad s⁻¹. Now, we must choose the Ω_1 and V_1 for ion trapping in a way that suppresses parametric heating of electrons. It is crucial to keep the electron's secular frequency higher than the driving frequency for ion confinement. Otherwise, the Ω_2 frequency field would be too slow to save an electron from parametric excitation. So another condition that must be satisfied in two frequency trapping is:

$$\Omega_1 \ll \omega_2 = \frac{QV_2}{\sqrt{2}M_{el}\ell_0^2\Omega_2} \approx 2.65 \times 10^9 \text{ rad s}^{-1}, \quad (2.7)$$

where the second equality follows from (1.38). Unfortunately [13], it is not possible to forestall parametric heating all the time. In the case of

$$\mu\Omega_1 = 2\omega_2,$$

where $\mu \in \mathbb{N}$, we can expect electrons' instability due to resonance of driving Ω_1 and secular ω_2 frequency. This estimation clarifies the origin of unstable tongues in stability diagrams; see 3 the last chapter.

We aim to create a Coulomb crystal and trap electrons within so that a cooled electron could spread its de Broglie wavelength across multiple ions. From (2.6) we see that it is possible to achieve plausible spring ratios by making the fraction Ω_1/Ω_2 small. However, we must not forget that lowering the frequency Ω_1 causes weaker confinement of both species. Intending to find a suitable middle ground, we chose Ω_1 such that $\Omega_2/\Omega_1 \approx 833$ and the corresponding spring constant ratio is $K \approx 42$.

2.2 Floquet theory

We are lucky to have a theory covering linear first-order ODEs with periodic coefficients, meaning the equations in the form:

$$\dot{\mathbf{u}}(\tau) = \mathbb{T}(\tau)\mathbf{u}(\tau), \quad (2.8)$$

where \mathbb{T} is a matrix valued function with minimal period T . Let's illustrate this theory for the case of our differential equation. We begin by rewriting the equation (2.2) as one general system of two first-order differential equations written in the matrix form:

$$\frac{d}{d\tau} \begin{bmatrix} \zeta(\tau) \\ \dot{\zeta}(\tau) \end{bmatrix} = \begin{bmatrix} 0 & 1 \\ \tilde{a} - 2\tilde{q}_1 \cos(2\tau\Omega_1/\Omega_2) - 2\tilde{q}_2 \cos(2\tau) & 0 \end{bmatrix} \begin{bmatrix} \zeta(\tau) \\ \dot{\zeta}(\tau) \end{bmatrix}, \quad (2.9)$$

where:

$$\zeta \in \{x, y, z\}, \quad (2.10)$$

$$\{\tilde{a}, \tilde{q}_1, \tilde{q}_2\} = \begin{cases} \{a, q_1, q_2\} & \text{if } (\zeta = x) \vee (\zeta = y), \\ -2\{a, q_1, q_2\} & \text{if } (\zeta = z). \end{cases} \quad (2.11)$$

This system (2.9) already has a structure of (2.8). Without the necessity of finding a solution to this system, we can acquire knowledge about its stability. The information we are interested in is whether a solution is bounded for a given set of parameters or not. In this section, we will limit ourselves to the driving frequencies, which can be represented as: $\Omega_2/\Omega_1 \equiv m/n$, where m and n are integers and m/n is an irreducible fraction. Then the matrix in equation (2.9) is $T = m\pi$ periodic. As in [7], we identify the edge of stability regions as a set of parameters for which a solution of (2.9) is a T or $2T$ periodic function¹. This allows us to seek a solution to our problem in the form:

$$\zeta(\tau) = \sum_{k=-\infty}^{\infty} c_k \exp\left(i \frac{k}{m} \tau\right), \quad (2.12)$$

where c_k are constant coefficients. Substituting this into equation (2.9) yields an identity:

$$\sum_{k=-\infty}^{\infty} \left[\left(\tilde{a} - \frac{k^2}{m^2} \right) c_k - \tilde{q}_1 (c_{k-2n} + c_{k+2n}) - \tilde{q}_2 (c_{k-2m} + c_{k+2m}) \right] \exp\left(i \frac{k}{m} \tau\right) = 0, \quad (2.13)$$

which holds for every τ only if each element of the sum is equal to zero. This relation can be written as:

$$\mathbb{F} \cdot \begin{bmatrix} \vdots \\ c_{k-1} \\ c_k \\ c_{k+1} \\ \vdots \end{bmatrix} = \mathbf{0}, \quad (2.14)$$

¹Note that such stability condition differs from the one we demand while simulating the motion of a particle. The periodic solution of equation of motion implies boundedness, but the value of this boundary might lie outside the physical dimensions of the trap. That is why we ought not to be surprised when we find some differences in stability diagrams, even for the simplest case of a single particle in the trap.

where \mathbb{F} is an infinite matrix with elements:

$$\mathbb{F}_{ij} = \left[\left(\tilde{a} - \frac{k^2}{m^2} \right) \delta_{ij} - \tilde{q}_1 (\delta_{ij-2n} + \delta_{ij+2n}) - \tilde{q}_2 (\delta_{ij-2m} + \delta_{ij+2m}) \right], \quad (2.15)$$

where:

$$\delta_{ij} = \begin{cases} 1 & i = j, \\ 0 & i \neq j. \end{cases} \quad (2.16)$$

The equation (2.14) is equivalent to:

$$\det(\mathbb{F}) = 0. \quad (2.17)$$

So the determination of stability boils down to computing a determinant of a matrix \mathbb{F} . We approximate \mathbb{F} by sufficiently large $\rightarrow (10m + 1) \times (10m + 1)$ finite matrix. For the index k in previous equations it means:

$$k \in \{-5m, -5m + 1, \dots, 5m - 1, 5m\} \subset \mathbb{Z},$$

neglecting solutions with smaller periods. Parameters for which $\det(\mathbb{F}) > 0$ were identified as stable and for $\det(\mathbb{F}) < 0$ as unstable. Since the particle experiences the most instabilities in the z -direction, we focus on the case $\zeta = z$ in the determinant solutions in the last chapter 3.

2.3 Simulation

Let us begin this section by summarizing our approximations, some of which we have already applied while deriving the equation of motion. We follow mainly the overview from [15]. Starting with insignificant neglections and moving towards more problematic ones.

Gravitational interaction: neglecting gravitational interaction goes without saying since, for Ca+ ions, it is weaker than electrostatic force by order of $\sim 10^{32}$.

Relativistic effects: we did not involve any relativistic corrections since we usually deal with small velocities while trapping particles. Ca+ ions are Doppler cooled down to energies of $\sim 10^{-4}$ eV. The fastest simulated electrons had a kinetic energy of ~ 1 eV, for which the relativistic gamma factor is still $\gamma \approx 1$ up to the fifth decimal place.

Ion radiation: a well-known consequence of Maxwell equations is that accelerating charged particle emits electromagnetic radiation. The power $[P] = [\text{Watt}]$ of such radiation can be for our non-relativistic case calculated using [16] the Larmor formula:

$$P = \frac{Q^2 a_c^2}{6\pi\epsilon_0 c^3},$$

where c is a speed of light, a_c denotes the acceleration of a particle at the given time, and ϵ_0 is the vacuum permittivity. We can estimate this radiation power for electron by taking an average² value of it's acceleration during stable trajectories from our simulations: $\langle a_c \rangle \sim 1 \times 10^{17} \text{ m s}^{-2}$. The resulting radiation power is then: $\langle P \rangle \approx 5 \times 10^{-20} \text{ W}$ which has, in the timescale of our simulations $\sim 10^{-7} \text{ s}$ a negligible effect. Radiation power for ions would be even less significant.

Electromagnetic field: Let us begin by writing full form Maxwell's equations assuming we can provide sufficient vacuum to disregard material properties:

$$\nabla \cdot \mathbf{E} = \frac{\rho}{\epsilon_0}, \quad (2.18a)$$

$$\nabla \times \mathbf{E} = - \frac{\partial \mathbf{B}}{\partial t}, \quad (2.18b)$$

$$\nabla \cdot \mathbf{B} = 0, \quad (2.18c)$$

$$\nabla \times \mathbf{B} = \frac{1}{c^2} \left(\frac{\mathbf{j}}{\epsilon_0} + \frac{\partial \mathbf{E}}{\partial t} \right), \quad (2.18d)$$

where ρ is a charge density and \mathbf{j} is current density. We are using quasistatic approximation instead:

$$\nabla \cdot \mathbf{E} = 0, \quad (2.19a)$$

$$\nabla \times \mathbf{E} = \mathbf{0}, \quad (2.19b)$$

$$\nabla \cdot \mathbf{B} = 0, \quad (2.19c)$$

$$\nabla \times \mathbf{B} = \mathbf{0}. \quad (2.19d)$$

We are setting $\rho = 0$ because we derive our equations in charge-free space. The Coulomb interaction is included in the simulation afterwards, exploiting the linearity of Maxwell's equations. The current density inside

²Average value defined as: $\langle \xi \rangle = 1/T \int_0^T \xi(\tau) d\tau$, where T denotes a total time of simulation.

our trap caused by a moving electron with maximal speed throughout our simulations $v_{\max} \sim 10^4$, can be estimated as:

$$j = \rho v \approx Qv/\ell_0^3 \sim 10^{-4} \text{ A m}^{-2}. \quad (2.20)$$

Overall, the amplitude of an oscillating magnetic field is much smaller than that of an electric [15]: $E_0/B_0 = c$. This means that for a magnetic field to play any significant role in the equation of motion, the particle would have to have a speed comparable to the speed of light, which is not the case, as we have already discussed. Even though we are not using any external magnetic field, the validity of equation (2.19b) requires one more condition [15] for a wavelength of our changing electric field, and that is:

$$\lambda \equiv \frac{2\pi c}{\Omega_2} \gg \ell_0, \quad (2.21)$$

after substituting corresponding values we get: $\lambda = 100 \text{ mm} \gg 0.5 \text{ mm} = \ell_0$. If this condition was not met, there could be a possibility of forming standing waves that could change the trap's dynamics.

Induced charge on the electrodes: charged particles induce surface charge density on the electrodes. This causes attraction of a particle toward the electrode, which can contribute to vacation of the particle from the trap. For a reference, we can look at simplified situation of a charged particle near an infinite conductive plane. As we have already stated, an average acceleration of the electron throughout the stable simulated trajectory was approximately $\langle a_c \rangle \sim 10^{17} \text{ m s}^{-2}$. For an infinite plane to cause an acceleration $\sim \langle a_c \rangle / 100$, the electron would have to approach the electrode up to the distance of $\approx 0.25 \mu\text{m}$, which would already be outside our definition of stable trajectory. Hence we can omit such an effect.

Creation of Rydberg atoms: an electron can get caught in some highly excited ion orbital creating a Rydberg atom. The electron can subsequently drop to a lower but still volatile state and vacate from it under the influence of the trap, losing energy by the associated photon emission. An electron moving inside a Coulomb crystal can be within reach of multiple ions simultaneously. Hence it may greatly contribute to electron cooling. It will be necessary to add such a process to our simulation in the future.

Phase shift: is caused by the finite speed of electric signal delivered to the electrode. This could be problematic since the characteristic dimension of our trap is $\ell_0 = 0.5 \text{ mm}$, and we are using frequencies up to the orders of $\Omega_2 \sim 10^{10} \text{ rad s}^{-1}$. We tackle this problem by dividing our electrodes into eight sections, see 1.2a, each with its own feeding from the power source.

Imperfection of electrodes: adding some perturbation to the electric potential caused by the imperfection of electrodes and the following study of its impact on stability will be one of the subjects for our future research.

Collisions with neutrals: we will be able to make a vacuum with pressure of $P \sim 10^{-13}$ bar. At this pressure, the heaviest remaining gas component is helium atoms. The collision frequency z is defined as:

$$z = \frac{Z}{V} = \frac{N_{el} N_{He}}{V} \sigma \sqrt{\frac{8k_b T}{\pi \mu}}, \quad (2.22)$$

where N_{el} and N_{He} are electron and helium counts respectively, μ is a reduced mass, σ is the collision cross-section, and V is a volume of the gas. The reduced mass for an electron and a helium atom is:

$$\mu = \frac{M_{el} M_{He}}{M_{el} + M_{He}}. \quad (2.23)$$

Looking at helium as an ideal gas in thermodynamic equilibrium, we can derive the number of helium atoms as:

$$N_{He} = \frac{PV}{k_b T}. \quad (2.24)$$

The number of electrons will be in the orders of $N_{el} \sim 1$. We can approximate electron-helium collision as a collision of hard spheres. In that case, the cross-section is equal to $\sigma \approx \pi r_w^2$, where r_w is a van der Waals radius³ of a helium atom: $r_w = 2.31 \times 10^{-10}$ m. Assuming room temperature $T = 300$ K helium gas, we get a final collision frequency:

$$z = r_w^2 P \sqrt{\frac{8\pi}{\mu k_b T}} \approx 4.36 \times 10^{-2} \text{ Hz}, \quad (2.25)$$

which means that we could observe such collisions in our experiment. However, the occurrence of these collisions is very unlikely in the time scales of our simulations; hence we do not include them. Nevertheless, as we will show, these collisions could affect long-term electron stability. It is not hard to prove that in the case of solid spheres, the change in a helium's kinetic energy after one elastic collision with an electron is:

not 100% sure whether this is correct

$$\frac{\Delta E_k^{He}}{E_k^{He}} = -2 \frac{M_{el} M_{He}}{(M_{el} + M_{He})^2} (1 - \cos \chi) = -\frac{\Delta E_k^{el}}{E_k^{He}}, \quad (2.26)$$

³In the hard sphere model, van der Waals radius indicates a radius of an atom.

where χ is a dispersion angle. The maximal change in kinetic energy happens for $\chi = \pi$. Considering helium atoms at a room temperature $T = 300\text{ K}$, the value of this energy change is $\Delta E = 0.16\text{ K}$, which would be enough to kick a weakly confined electron out of the trap⁴.

2.3.1 Choice of time-step

When looking at the electrons' stability, we use a total simulation length corresponding to twenty secular oscillations ($20/\omega$) (1.38), if we do not say otherwise. When examining the average velocity of an electron, it was sometimes necessary to extend this time up to two-hundred secular oscillations to harvest the practically relevant information. Choice of time-step is always a delicate issue. We used a constant time-step to solve differential equations with the explicit time dependency, following the Nyquist criterion [17]. Nyquist criterion is used mainly in processing compact signals with convergent Fourier series. It states that for the signal with the highest frequency $f \equiv \Omega/2\pi$, the largest possible sample size so that the discretization of the signal will carry equivalent information as the continuous one is $1/(2f)$. We started numerically solving the equation of motion with this time step, gradually decreasing its size until the numerical solution with the denser sampling would give us the same result for the given tolerance. Repeating this process for several numerical methods [18] for integrating ODEs. For the case of a single electron in the trap had the best performance a predictor-corrector method. The sufficient time-step was $\Delta t = 1/(10\Omega)$. For simulations including multiple particles, we have used a Verlet method with an adaptive time-step.

2.3.2 Treatment of laser cooling

In our simulation, we treated the laser cooling of ions by introducing a frictional force⁵. The strength of this force is characterized by the parameter $\beta \in (0, 1)$.

2.3.3 Simulating Coulomb crystal

We simulated Coulomb crystal by molecular dynamics, meaning we solved the equation of motion for each ion in effective potential, including Coulomb interactions and damping. The damping parameter β was chosen large enough to decelerate the particles within a computationally reasonable time. To ensure that the ions had enough time to find a potential minimum, they were given a

⁴In our experiment, we will be able to create a potential well for ions with a maximum depth of 32 mK , and for electrons with maximal depth up to 15 K .

⁵Meaning a force proportional to $\propto -\dot{\mathbf{r}}$.

synthetic boost in kinetic energy every time their temperature reached below 0.01 Kelvin.

2.3.4 The code

The practical part of this thesis consists of developing the code simulating the motion of ions and electrons in a two frequency Paul trap. We have chosen the programming language python for its current popularity allied with an abundance of highly optimized libraries, and a good combination of computational and development costs. The source code can be found at github⁶. Main features of the program are:

- Creating a Coulomb crystal.
- Making stability diagram in dependence on q_1 and q_2 parameters.
- Parallelizing the computation of stability diagram.
- Optimizing the algorithm to compute stability only on the edge of stability regions.
- Tracking the information about the system: positions, velocities, energies
- Producing graphical outcomes.

More about its functionalities can be found in the appendix A.1.

⁶https://github.com/rendeka/Bachelor_thesis.git

Chapter 3

Results and discussion

3.1 Characteristics of q_1 - q_2 stability diagrams for one electron

We will start by looking at the stability diagrams for different Ω_2/Ω_1 ratios. Starting with 3.1.

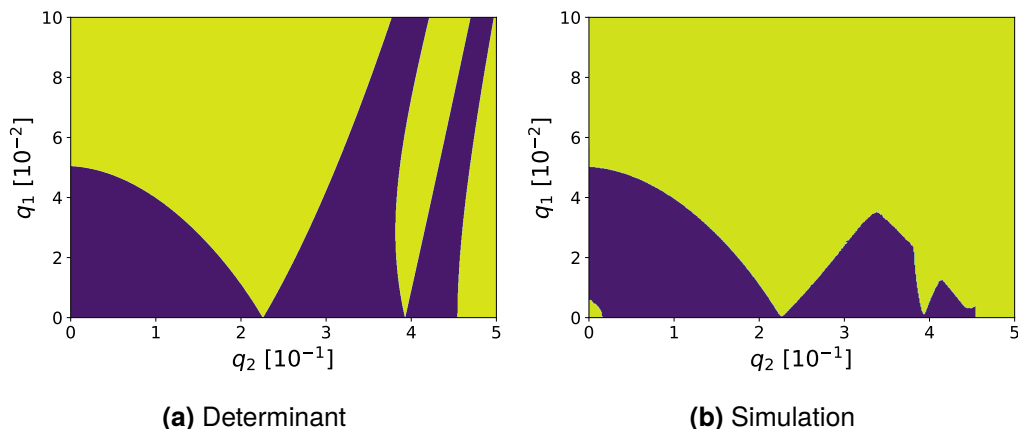


Figure 3.1 Stability diagrams for $\Omega_2/\Omega_1 = 3$

In the figure 3.1 we can see regions of stable(*dark*) and unstable(*light*) solutions to our equation of motion. The picture 3.1a was determined with use of Floquet theory. The adjacent image shows the stability of an electron based on numerical simulation. In contrast with the determinant solution, we can see some evident distinctions. The region around $q_1 \approx q_2 \approx 0$ became unstable. This is no surprise since in a weak field was not satisfied the stability requirement (1.44) for the given initial conditions. More importantly, two whole stability areas have melted

away in the field with higher amplitudes. We must not forget that the stability in the figure 3.1a is calculated only along the z-axis. We can investigate this by setting the initial position and velocity in x-y directions to zero. As we can see, the subsequent picture 3.2a already agrees with the determinant solution 3.1a.

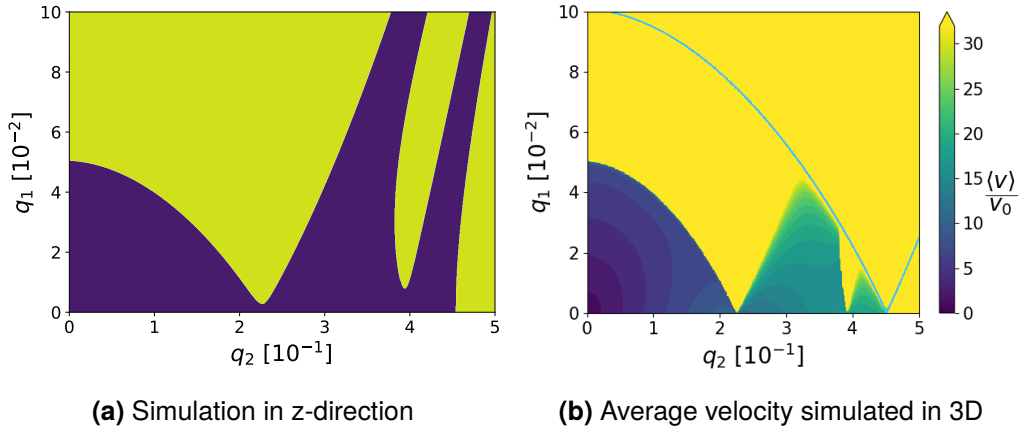


Figure 3.2 Stability diagrams for $\Omega_2/\Omega_1 = 3$

In the next set of pictures 3.3, we evaluate the stability diagram in x-y directions by setting $\zeta = x$ in (2.11) for a determinant solution and setting the z-component of initial position and velocity to zero in the simulation. The red trace in both pictures embodies the edge of stability made with our standard (1.45) stability requirement in simulation. The contour plot in 3.3b was created with the enhanced condition for identifying stable solutions from the standard (1.45) to $\max_{x \in \mathcal{L}}(r) \leq 2 \ell_0$, while increasing the total simulation time as well. So this picture 3.3b, among other things, illustrates the non-equivalence of our stability condition while simulating and the condition of stability we use in Floquet theory, as we have already mentioned in 1.

In the background of 3.2b is a contour plot of the average electron velocity $\langle v \rangle$ throughout the whole trajectory¹ relative to the initial velocity v_0 . The color bar to the right indicates the value of this ratio. We create all the other figures similar to 3.2b in the same way. These diagrams can help us find stable trap parameters while keeping electron temperature as low as possible, which is our ultimate goal. The light blue line in 3.2b represents the stability edge taken from 3.3, delivering a crucial message about the difference between the two stability diagrams in 3.1. We see that our discrepancy problem between determinant and simulated stability diagrams is settled by the obvious necessity to combine determinant solutions in both x and z directions. This can be easily fixed with the cost of doubling the

¹Average value defined as: $\langle \xi \rangle = 1/T \int_0^T \xi(\tau) d\tau$, where T denotes a total time of simulation.

computation time for a determinant solution. Nonetheless, from now on, we will focus on simulated results, keeping the determinant diagrams in the z-direction for comparison. Moreover, we can use these pictures 3.3 as a sanity check. By matching them with the results from [7] (*where the stability of the ideal quadrupole trap along the x-direction was studied*), we see that we have reproduced the same² results → proving the validity of our code, at least to some extent.

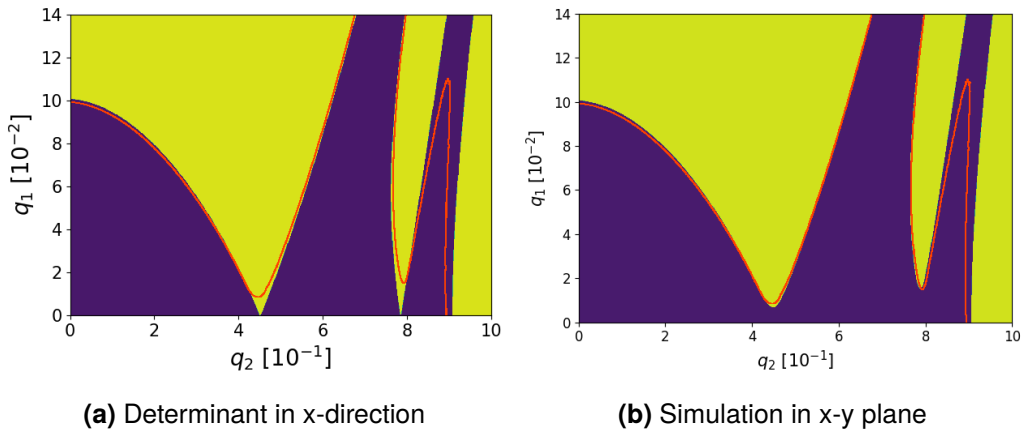


Figure 3.3 Stability diagrams for $\Omega_2/\Omega_1 = 3$ in x-y plane

The image 3.4 again combines two pictures. The pink curve from now on construes the stable simulated regions, in this case, taken for 3.1b.

²Note that we are using different condition to identify stable solutions.

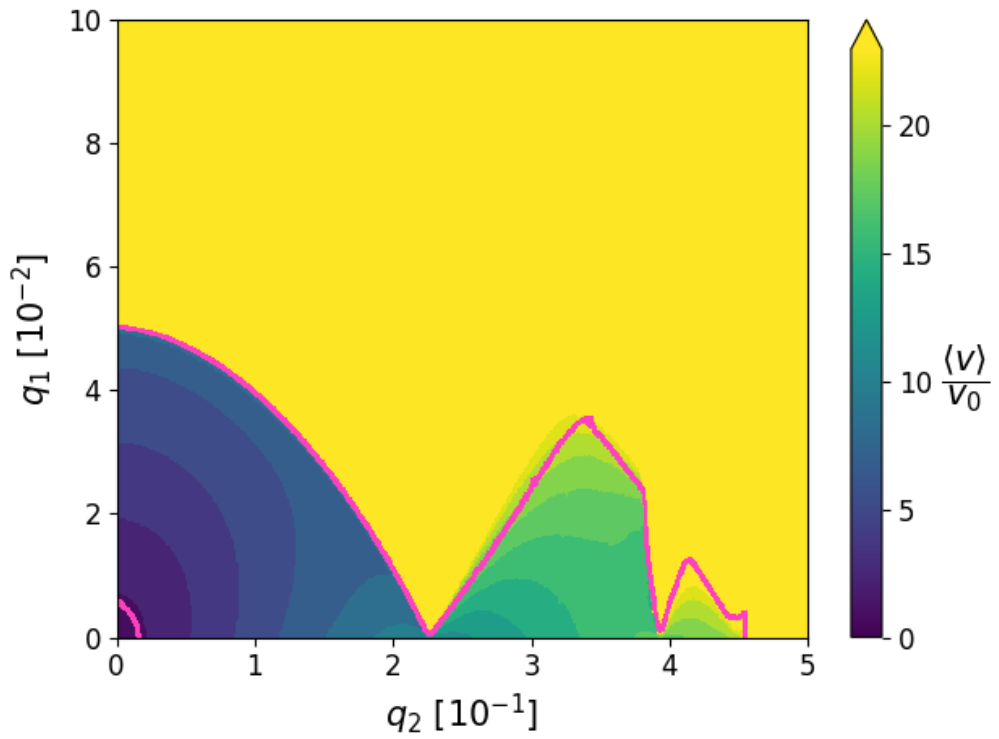


Figure 3.4 Average electron velocity for $\Omega_2/\Omega_1 = 3$

Moving to larger frequency ratio $\rightarrow \Omega_2/\Omega_1 = 13$ we can start to notice some patterns.

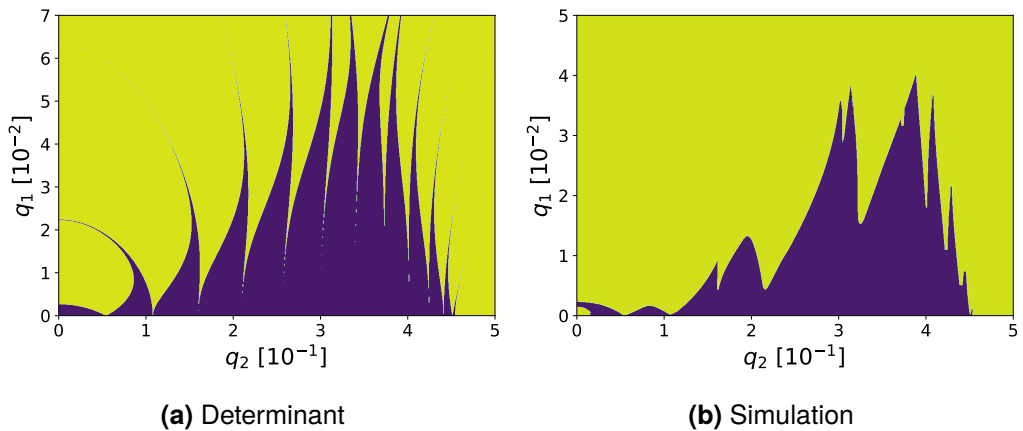


Figure 3.5 Stability diagrams for $\Omega_2/\Omega_1 = 13$

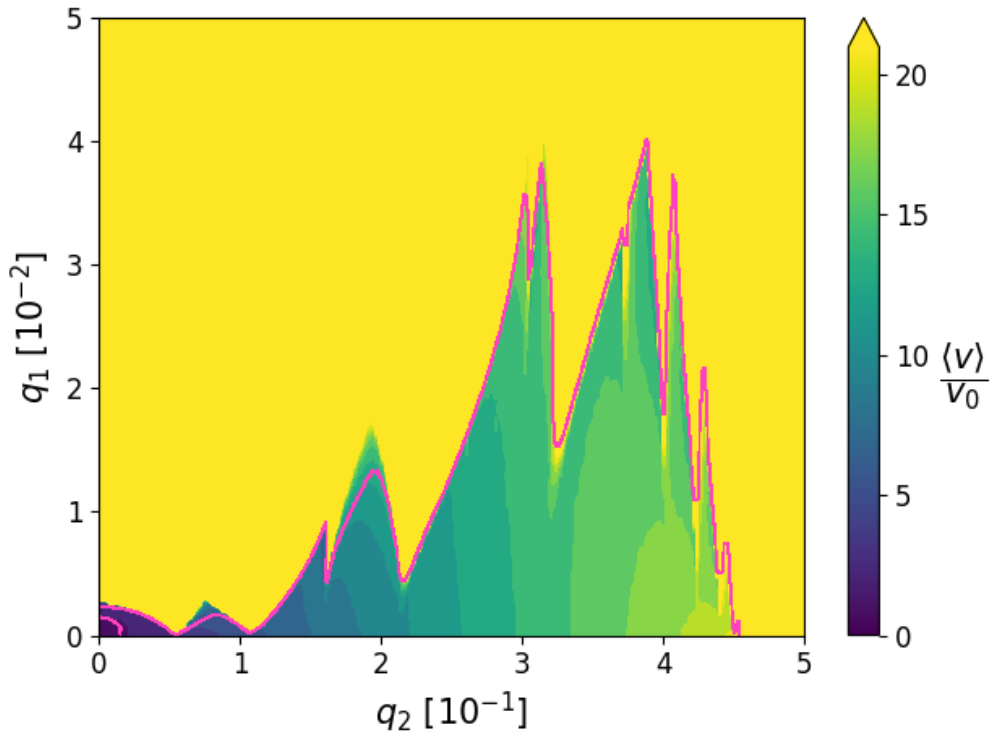


Figure 3.6 Average electron velocity for $\Omega_2/\Omega_1 = 13$

There emerges one stable triangle with many tongues of instability. With an increasing ratio Ω_2/Ω_1 we can see a gain in the number of these tongues, but their width promptly shrinks as well. We expect that by further increasing the frequency ratio, the unstable tongues will be realistically affecting only the regions near the edge of stability, leaving the regions further inside a stable triangle safe to work with.

Continuing to the frequency ratio compatible for trapping electrons and Ca+ ions $\rightarrow \Omega_2/\Omega_1 = 833$

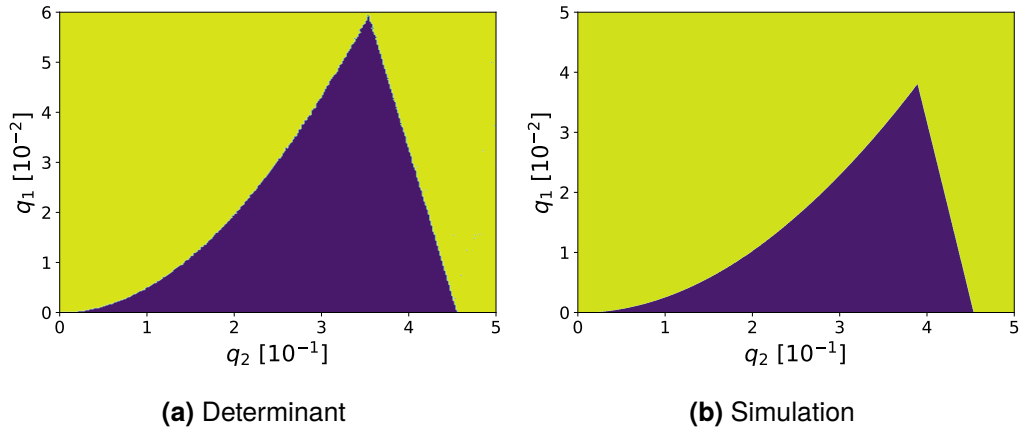


Figure 3.7 Stability diagrams for $\Omega_2/\Omega_1 = 833$

At this point, the unstable tongues became so dense and narrow that we practically could not see them in stability diagrams 3.7. The closeup on the stability edge 3.9 was evaluated after a thousand secular oscillations, and the tongues vanished virtually instantly. The stability triangle will continue to shrink with an increasing frequency ratio. However, the character of this region will stay the same. Therefore, predicting stability for different frequency ratios in this range is forthright.

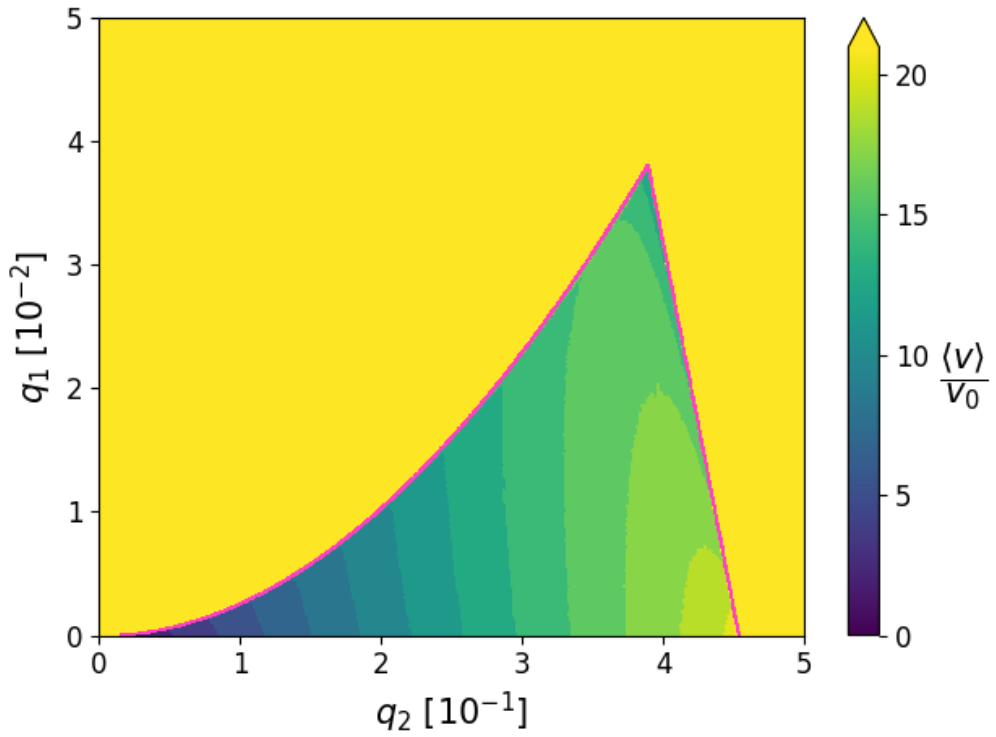


Figure 3.8 Average electron velocity for $\Omega_2/\Omega_1 = 833$

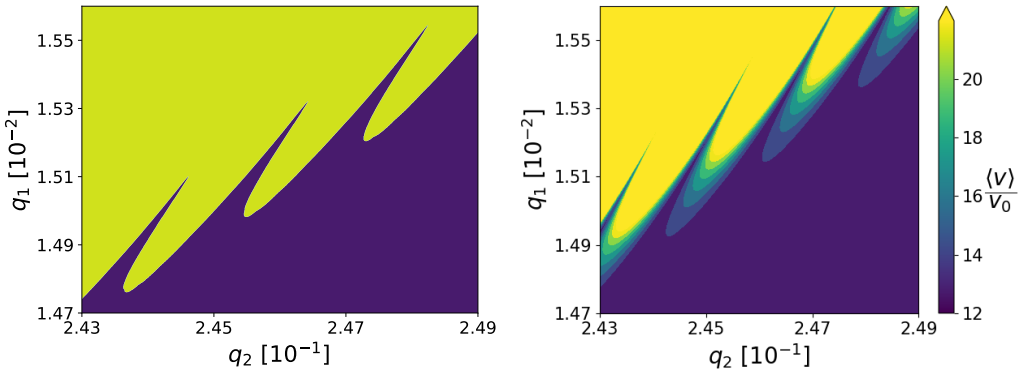


Figure 3.9 Simulated edge of stability for $\Omega_2/\Omega_1 = 833$

The essential information comes from the figure 3.8. As we can see, an electron's average velocity drops in weaker fields, furnishing us with a method to reach lower electron velocities. Imagine we have already set up a CC and managed

to trap an electron inside it. Assuming the electron can cool itself by interactions with ions, we can follow by gradual change of trapping parameters aiming towards the weak field region, effectively lowering the electrons' temperature. Such a process will be simulated in the future.

It is worth pointing out that the computation time of the determinant stability diagram already exceeds that of simulated for a frequency ratio this big. However, we apply a built-in NumPy³ function for computing determinants using LU decomposition [18] with time complexity $\mathcal{O}(n^3)$, not utilizing the fact that our matrices are sparse. Moreover, we are interested only in the sign of a determinant which also supports a capacity for efficiency improvement. But since the determinant solutions are not essential to us, we do not investigate such further advancements in this thesis.

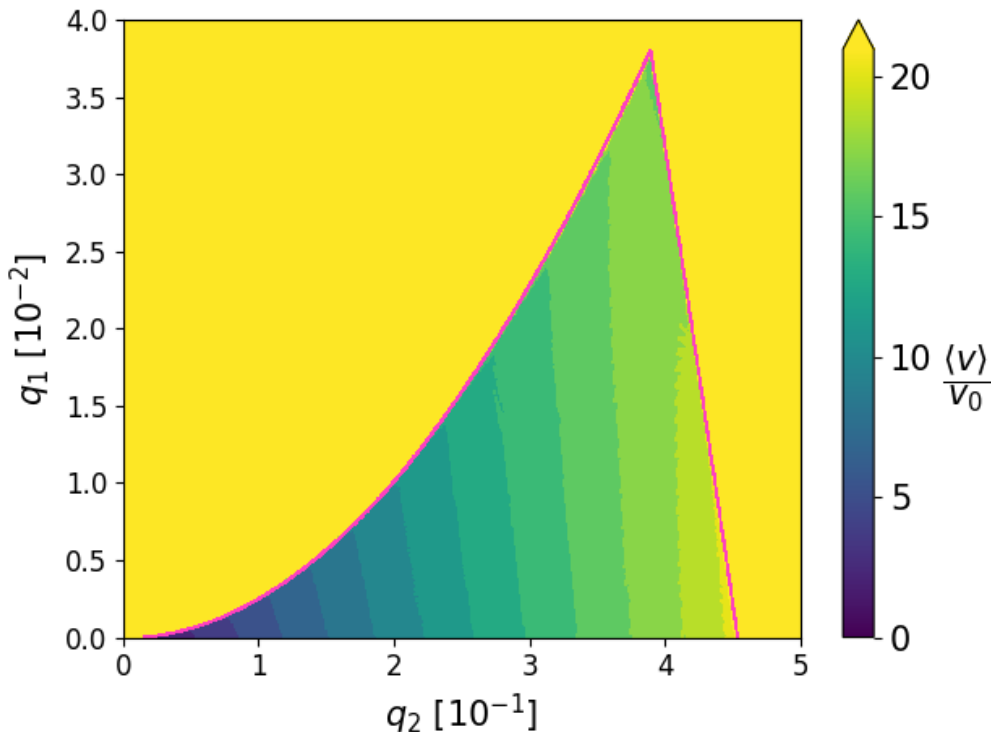


Figure 3.10 Average electron velocity for $\Omega_2/\Omega_1 = 1207$

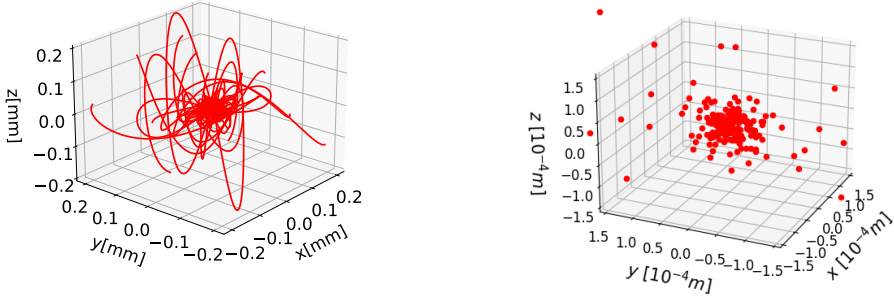
We produced one more diagram showing stability and average electron velocity for the different ratio of driving frequencies. As was predicted, solutions with lower frequency ω_1 are less stable but show similar qualities as 3.8.

³NumPy is widely used, open source, numerical python library: <https://numpy.org/>

3.2 Creating a Coulomb crystal

As we have already mentioned, we assemble a CC by solving the equation of motion for each ion in an effective potential with damping and mutual Coulombic interaction. Meaning that the equation of motion for the i -th ion takes the form:

$$M_{\text{ion}} \ddot{\mathbf{r}}_i = \sum_{\substack{j=1 \\ j \neq i}}^N \frac{Q^2}{4\pi\epsilon_0} \frac{\mathbf{r}_i - \mathbf{r}_j}{|\mathbf{r}_i - \mathbf{r}_j|^3} - \frac{M_{\text{el}}^2 \Omega_2^2}{8M_{\text{ion}}} \left((\Omega_2/\Omega_1)^2 q_1^2 + q_2^2 \right) \begin{bmatrix} x_i \\ y_i \\ 4z_i \end{bmatrix} - \beta \dot{\mathbf{r}}_i \quad (3.1)$$



(a) Simulating multiple ions in effective potential with damping (b) Process of assembling a CC (200 ions)

Figure 3.11 Creating CC $\Omega_2/\Omega_1 = 1207$

3.3 Stability of electron in Coulomb crystal

The ions stand practically still in the time scales in orders of ~ 10 secular electron oscillations. Therefore, while computing stability diagrams in the presence of CCs, we freeze ions in place, rapidly improving computational time. We have performed such simulations with up to 200 ions, solving the equation for a i -th electron in the variable $\tau = t\Omega_2/2$:

$$\ddot{\mathbf{r}}_i = \frac{Q^2}{\pi M_{\text{el}} \epsilon_0 \Omega_2^2} \left(\sum_{\substack{j=1 \\ j \neq i}}^{N_j} \frac{\mathbf{r}_i - \mathbf{r}_j}{|\mathbf{r}_i - \mathbf{r}_j|^3} - \sum_{k=1}^{N_k} \frac{\mathbf{r}_i - \mathbf{R}_k}{|\mathbf{r}_i - \mathbf{R}_k|^3} \right) - \left(a - 2q_1 \cos(2\tau\Omega_1/\Omega_2) - 2q_2 \cos(2\tau) \right) \begin{bmatrix} x \\ y \\ -2z \end{bmatrix}, \quad (3.2)$$

where r_j denotes a position of j -th electron, and R_k is the constant position of k -th ion. N_j and N_k are the total numbers of electrons and ions respectively. We have simulated stability diagrams by solving equation (3.2) with up to 200 ions and frequency ratios $\Omega_2/\Omega_1 = 833$ and $\Omega_2/\Omega_1 = 1207$. However, we did not observe any noticeable differences from results obtained in the previous section 3.1. Nevertheless, instabilities may arise on longer time scales, which we did not manage to inspect in detail in this thesis, but will be investigated further.

3.4 Future

Our future concerns will begin by continuing the study of electrons' stability in the presence of CC on longer time scales and adding the option of electron cooling via interactions with ions. Another leap will be reproducing the results of this thesis for the real planar geometry of the trap used in our experiment. The potential of such a trap can be formulated in integral form utilizing Bessel functions, making our simulations much more computationally expensive. We need to derive the equation of motion and identify parameters analogous to a , q_1 , and q_2 , which we had for the ideal quadrupole trap. After that, we can use our exiting program to study the stability and average particle velocity in dependence on such parameters exactly as we did in this thesis.

Conclusion

In this thesis, we have proposed a design of an experiment offering the possibility of assembling a stable Coulomb crystal with electrons trapped inside it. We are aiming to achieve cooling of electrons up to the point when they form a Fermi gas. If successful, such an experiment would expand current lines of research on quantum systems.

We have presented a comprehensive overview of the current state of knowledge regarding the trapping of charged particles solely by an electric field. We have shown the general treatment of effective potential and stability, using it on the concrete case of the ideal Paul trap, for which we have derived equations of motion. Based on pseudopotential approximation, we have exhibited the supremacy of trapping with two frequencies instead of one for the confinement of two species with widely different charge-to-mass ratios.

We have developed a computer program for simulating charged particles inside the Paul trap. Using this script, we studied the stability of particles in dependence on the trap settings, identifying whole areas of stable operating conditions. By reproducing results for trapping in one direction from reviewed scientific articles, we have confirmed the validity of our simulations. After that, we continued producing novel results by studying the stability of electrons in all spatial directions. Other than stability, we evaluated an average electron velocity throughout the trajectory dependent on the trap parameters. We have found that low electron temperatures could be achieved in the weaker electric fields. Based on these results, we propose a technique to achieve successful electron cooling by the successive change of trapping parameters. To model such a process, we must add a feature to our program representing electrons' possibility to cool themselves by interaction with ions. The program will be further developed for use in the real geometry of our trap.

Bibliography

- [1] S. Earnshaw. “On the nature of the molecular forces which regulate the constitution of the luminiferous ether”. In: *Transactions of the Cambridge Philosophical Society* 7 (1848), p. 97.
- [2] M. Drewsen et al. “Ion Coulomb crystals: a tool for studying ion processes”. In: *International Journal of Mass Spectrometry* 229.1-2 (2003), pp. 83–91.
- [3] R. C. Thompson. “Ion coulomb crystals”. In: *Contemporary Physics* 56.1 (2015), pp. 63–79.
- [4] R. Fitzpatrick. *Plasma physics: an introduction*. Crc Press, 2014.
- [5] D. Gerlich. “Inhomogeneous rf fields: a versatile tool for the study of processes with slow ions”. In: *Advances in chemical physics* 82 (1992), pp. 1–176.
- [6] S. Fanghänel, O. Asvany, and S. Schlemmer. “Optimization of RF multipole ion trap geometries”. In: *Journal of Molecular Spectroscopy* 332 (2017). Molecular Spectroscopy in Traps, pp. 124–133. ISSN: 0022-2852. doi: <https://doi.org/10.1016/j.jms.2016.12.003>.
- [7] N. Leefer et al. “Investigation of two-frequency Paul traps for antihydrogen production”. In: *Hyperfine Interactions* 238.1 (2017), pp. 1–18.
- [8] R. Coisson, G. Vernizzi, and X. Yang. “Mathieu functions and numerical solutions of the Mathieu equation”. In: *2009 IEEE International Workshop on Open-source Software for Scientific Computation (OSSC)*. 2009, pp. 3–10. doi: [10.1109/OSSC.2009.5416839](https://doi.org/10.1109/OSSC.2009.5416839).
- [9] N. P. Bhatia and G. P. Szegö. *Stability theory of dynamical systems*. Springer Science & Business Media, 2002.
- [10] A. M. Lyapunov. “The general problem of the stability of motion”. In: *International journal of control* 55.3 (1992), pp. 531–534.
- [11] S Urabe et al. “Laser cooling of a single Ca^+ ion: observation of quantum jumps”. In: *Applied Physics B* 57.5 (1993), pp. 367–371.

- [12] J. C. Foot. *Atomic physics*. eng. Oxford master series in physics. Atomic, optical, and laser physics ; Oxford master series in physics., Atomic, optical, and laser physics. Oxford: Oxford University Press, 2005. ISBN: 0-19-850696-1.
- [13] C. Foot et al. “Two-frequency operation of a Paul trap to optimise confinement of two species of ions”. In: *International Journal of Mass Spectrometry* 430 (2018), pp. 117–125. ISSN: 1387-3806. doi: <https://doi.org/10.1016/j.ijms.2018.05.007>.
- [14] D. Trypogeorgos and C. J. Foot. “Cotrapping different species in ion traps using multiple radio frequencies”. In: *Physical Review A* 94.2 (2016), p. 023609.
- [15] M. H. Friedman, A. L. Yergey, and J. E. Campana. “Fundamentals of ion motion in electric radio-frequency multipole fields”. In: *Journal of Physics E: Scientific Instruments* 15.1 (1982), pp. 53–56. doi: 10.1088/0022-3735/15/1/010.
- [16] J. Larmor. “LXIII. On the theory of the magnetic influence on spectra; and on the radiation from moving ions”. In: *The London, Edinburgh, and Dublin Philosophical Magazine and Journal of Science* 44.271 (1897), pp. 503–512.
- [17] C. Shannon. “Communication in the Presence of Noise”. In: *Proceedings of the IRE* 37.1 (1949), pp. 10–21. doi: 10.1109/JRPROC.1949.232969.
- [18] S. A. Teukolsky et al. “Numerical recipes in C”. In: *SMR* 693.1 (1992), pp. 59–70.

Appendix A

Using software

We have performed our calculations on a cluster with 32GiB of RAM, the 24-core processor: 12th generation Intel Core i9-12900KF. The program is not optimized for minimal memory usage, and it is possible that some procedures will not run successfully on the less powerful machines.

A.1 Python script

We do not provide an entire architecture of our program since it awaits an extensive reconstruction in the near future. In this appendix, we explain how to use the basic functionalities of the developed python script. Of course, it is best to follow actualized instructions on the github¹. The program starts by running the `main.py` file. This file has definitions of functions using many different modules. When running the `main.py`, one should uncomment all the lines he/she wants to be executed. Fixed parameters can be adjusted in the module `parameters.py`.

¹https://github.com/rendeka/Bachelor_thesis.git

